PROCEEDINGS, Thirty-Sixth Workshop on Geothermal Reservoir Engineering
Stanford University, Stanford, California, January 31 - February 2, 2011

Discrete Element Modeling of Rock Deformation, Fracture Network Development and Permeability Evolution Under Hydraulic Stimulation

[1,2]Shouchun Deng, [3]Robert Podgorney, [2]Hai Huang
[1]University of Idaho
[2]Carbon Resource Management Department, Idaho National Laboratory
[3]Renewable Energy Technologies, Idaho National Laboratory
PO Box 1625
Idaho Falls, ID, 83415
e-mail: shouchun.deng@inl.gov

Abstract

A number of challenges are associated with engineered geothermal system (EGS) reservoir development, including the ability to reliably predict hydraulic fracturing, the deformation of natural fractures, and estimating permeability evolution of the fracture network with time. In order to research the behavior of EGS reservoirs, we have developed a three-dimensional discrete element method (DEM) rock deformation and fracturing model and coupled it with a network flow simulator in order to gain further understanding of these important processes. In DEM models, solid rock is represented by a network of discrete elements (often referred as particles) connected by various types of mechanical bonds such as springs, elastic beams or bonds that have more complex properties (such as stress-dependent elastic constants). Fracturing is represented explicitly as broken bonds (microcracks), which form and coalesce into macroscopic fractures when external and internal load is applied. Natural fractures are represented by a series of connected line segments. Mechanical bonds that intersect with such line segments are removed from the DEM model.

A network flow model using a conjugate lattice to the DEM network is also developed and coupled with the DEM. The fluid pressure gradient exerts forces on individual elements of the DEM network, which in turn deforms the mechanical bonds and breaks them if the deformation reaches a prescribed threshold value. Such deformation/fracturing changes the permeability of the flow network, which again provides feedback on the evolution of fluid pressure, intimately coupling the two processes. The coupling between fracture growth and deformation of existing fracture networks with fluid flow makes meso-scale DEM-network flow simulations necessary in order to accurately evaluate the permeability evolution, as these methods have substantial advantages over conventional continuum mechanical models of elastic rock deformation.

Introduction

Hydraulic fracturing can be understood as the process by which a fracture initiates and propagates due to hydraulic loading (i.e., pressure) applied by injecting a fluid inside the rock matrix/fracture system. The fractures exhibit complicated geometries, which reflect the complexity of the underlying physical mechanisms related to forming the hydraulic fractures in numerous rock types and stress regimes, at scales ranging from sub-millimeter to many kilometers. Even in its most basic form, hydraulic fracturing involves the coupling of at least three processes: (i) the mechanical deformation induced by the fluid pressure; (ii) the flow of fluid within the fracture; and (iii) the fracture propagation.

DEMs can directly mimic rock and thus exhibit a rich set of emergent behaviors that correspond very well with real rock. They also provide a tool to investigate the micro-mechanisms that combine to produce complex macroscopic behaviors or to predict these macroscopic behaviors (*Potyondy and Cundall, 2004*). In this paper, DEM is implemented to handle rock deformation and fracturing processes. Rock is viewed as circular / spherical particle cluster with finite mass, and its mechanical performance is represented by the stiffness and strength of particles or bonds between particles.

Considering that fluid flow is mainly within the fractures and fracture network, the permeability of the rock matrix can generally be omitted from network flow models. However, in order to simulate deformation and fracturing of the rock matrix blocks within which the fractures are embedded, the fluid

pressure from the fracture network is interpolated into the rock matrix blocks using a very simple form of the governing equations (linear algebraic). While this approach has significant limitations, and cannot fully describe all the dynamics involved with hydraulic stimulation, it has been adopted as an intermediate step in order to examine the governing physics and allow for incremental code development.

The coupling of fluid flow and rock deformation-fracture propagation, as stated above, is based on the assumption that the permeability of the rock matrix is sufficiently small that the fluid flow in matrix is negligible, yet it is large enough to propagate the pressure field in the rock matrix nearly instantaneously. This coupling includes the following two-way interaction:

(i) Change of fluid pressures on the particle surface affects the motion, and in turn, the deformation and propagation of fractures;
(ii) The change of fracture aperture affects their permeability, flow rate, and fluid pressure distribution along the fracture surface, i.e. the boundary surface tractions of particles, which, in turn, affects particle motion.

In this paper, we focus on the simulating the coupling fluid flow and particle movement. In the following sections, a brief introduction to DEM methodology will be presented, followed by a description of network flow and coupling, and numerical implementation issues. One numerical case is used to demonstrate the proposed solution strategy. Finally, we will discuss the merits and limitations of the proposed method, and point out the future work.

Modeling Theory

Here we introduce the theories of DEM, network flow models, and how to sequential couple the simulation of these two distinct processes.

DEM

The solid rock is treated as a cemented granular material of complex-shaped grains in which both the grains and the cements are deformable and may break (*Potyondy and Cundall, 2004*). For simplicity, the following assumptions are posed (Figure 1 illustrates its physical basis):

(1) The particles are circular or spherical rigid bodies with a finite mass for 2-dimensional or 3-dimensional cases, respectively.
(2) The particles move independently and can both translate and rotate.
(3) The particles interact only at contacts.
(4) The particles are allowed to overlap one another, and all overlaps are small relative to particle size.
(5) Bonds of finite stiffness can exist at contacts, and these bonds carry load and can break.

Because the DEM is formulated in a fully dynamical fashion, damping is necessary to dissipate kinetic energy, and the damping force F^d applied to each particle is given by

$$F^d = -\alpha \left|\vec{F}\right| sign\left(\vec{V}\right), \quad (1)$$

where α is dynamical damping, $\left|\vec{F}\right|$ and $\vec{V}$ are the total external force and velocity, respectively.

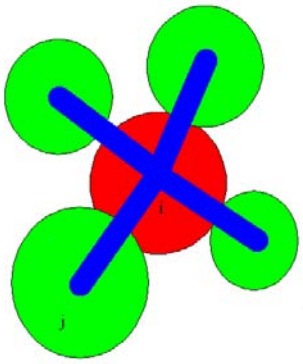

$$\begin{cases} F^n = K^n U^n \\ \Delta F^s = -K^s \Delta U^s \end{cases}$$

$$\begin{cases} Incremental\ normal\ force: \ \Delta \bar{F}^n = \bar{K}^n A \bullet \Delta U^n \\ Incremental\ shear\ force: \ \Delta \bar{F}^s = -\bar{K}^s A \bullet \Delta U^s \\ Incremental\ tortional\ moment: \ \Delta \bar{M}^n = -\bar{K}^s J \bullet \Delta \theta^n \\ Incremental\ bending\ moment: \ \Delta \bar{M}^s = -\bar{K}^n I \bullet \Delta \theta^s \end{cases}$$

Figure 1: Physical model of implemented DEM

For the interaction of two particles (grains), there are two types of force – normal and shear. The total normal force and the increment of shear force are calculated by (*Potyondy and Cundall, 2004*) as,

$$\begin{cases} F^n = K^n U^n \\ \Delta F^s = -K^s \Delta U^s \end{cases} \quad (2)$$

Here K^n and K^s denote the normal and shear stiffness between two grains, while U^n is the amount of overlap between the two (always positive); ΔU^s is the relative displacement at contact center between the two particles.

The shear force must satisfy the constraint condition,

$$\left|F^s\right| \le \mu F^n,$$
(3)

where $\mu = \min\left(\mu^{(A)}, \mu^{(B)}\right)$ is the friction coefficient of interaction, $\mu^{(A)}$ and $\mu^{(B)}$ are the friction coefficients of the two particles, respectively.

If we consider a rock grain with a cement layer to account for rock's tensile strength, there is a parallel bond – cement interaction between two adjacent particles. Cement interaction behaves as a spatial beam, and its constitutive equations are given as follows:

Incremental normal force:
$$\Delta\bar{F}^n = \bar{K}^n A \bullet \Delta U^n, \quad (4.a)$$

Incremental shear force:
$$\Delta\bar{F}^s = -\bar{K}^s A \bullet \Delta U^s, \quad (4.b)$$

Incremental torsional moment:
$$\Delta\bar{M}^n = -\bar{K}^s J \bullet \Delta\theta^n, \quad (4.c)$$

Incremental bending moment:
$$\Delta\bar{M}^s = -\bar{K}^n I \bullet \Delta\theta^s, \quad (4.d)$$

where A, J and I are the area, polar moment of inertia and moment of inertia of the parallel bond cross-section, respectively,

$$A = \begin{cases} 2\bar{R}t, t=1 & (2D) \\ \pi\bar{R}^2, & (3D) \end{cases}, \quad (5.a)$$

$$I = \begin{cases} \frac{2}{3}\bar{R}^3 t, t=1 & (2D) \\ \frac{1}{4}\pi\bar{R}^4, & (3D) \end{cases}, \quad (5.b)$$

$$J = \begin{cases} NA, & (2D) \\ \frac{1}{2}\pi\bar{R}^4, & (3D) \end{cases}, \quad (5.c)$$

and

$$\bar{R} = \bar{\lambda}\min\left(R^{(A)}, R^{(B)}\right), \quad (6)$$

where $R^{(A)}$ and $R^{(B)}$ are the radii of the two particles respectively. Generally the radius multiplier $\bar{\lambda} = 1$.

Cement interaction can break and never heal/reform as described below:

$$\begin{cases} \bar{\sigma}^{\max} = \dfrac{-\bar{F}^n}{A} + \dfrac{\left|\bar{M}^s\right|\bar{R}}{I} \le \bar{\sigma}_c \\ \bar{\tau}^{\max} = \dfrac{\left|\bar{F}^s\right|}{A} + \dfrac{\left|\bar{M}^n\right|\bar{R}}{J} \le \bar{\tau}_c \end{cases}, \quad (7)$$

where $\bar{\sigma}_c$ and $\bar{\tau}$ are the tensile and shear strengths, respectively.

Network Flow Model

The analysis of flow in the fracture network is based on three components; fracture segments, intersections and cycles. Intersections are the locations where two or more fractures meet and are the most important geometrical properties of a network for conducting flow. The part of a fracture between two adjacent intersections is called a segment and the set of fracture segments which form a complete block is called a fracture cycle, as shown in Figure 2.

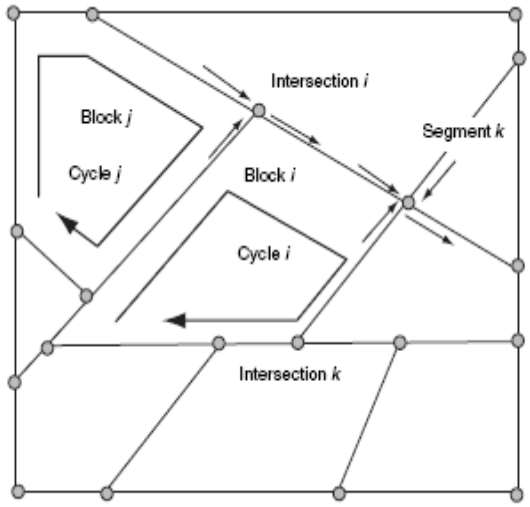

Figure 2: An idealized fracture network in 2D for flow analysis (Jing and Stephansson, 2007)

For the sake of our development, assume that there are n_i fracture segments connected at intersection i, where there also exists an external recharge (or discharge) rate q_i^s. Assuming fluid mass conservation and no changes in storage, the sum of total inflow rate and outflow rate should equal to the recharge (positive) or discharge (negative) rate (*Jing and Stephansson, 2007)*,

$$\frac{g\rho_f}{12\mu}\sum_{j=1}^{n_i}\left(e_{ij}\right)^3\frac{h_i-h_j}{L_{ij}}=q_i^s, \tag{8}$$

where h_i, h_j are the hydraulic heads at intersection i and j $(j=1,\cdots,n_i)$, ρ_f denotes fluid mass density, μ is the dynamic viscosity of the fluid and g is the gravitational acceleration. e_{ij} and L_{ij} are the equivalent hydraulic aperture size and length of the fracture segment between intersection i and j, respectively.

Generally, the fracture aperture size changes can be approximated using the porosity change,

$$e=e_0\left(\frac{\phi}{\phi_0}\right)^{\frac{3}{2}}, \tag{9}$$

where, e_0 denotes the initial aperture size. This relationship is derived from the cubic law between permeability and porosity changes (*Steefel and Lasaga, 1994*)

$$k=k_0\left(\frac{\phi}{\phi_0}\right)^3, \tag{10}$$

and the description of permeability in a plane parallel fracture (*Bear, 1992*)

$$k=\frac{e^2}{12}. \tag{11}$$

where, k_0, ϕ_0 are the initial permeability and local porosity, k and ϕ the current permeability and porosity, respectively.

For wedge-shaped fracture segments, the equivalent aperture size should be calculated by (*Jing and Stephansson, 2007*)

$$e_{ij}=\frac{e_i+e_j}{2}\left[\frac{16\left(e_i/e_j\right)^2}{\left(1+\left(e_i/e_j\right)\right)^4}\right], \tag{12}$$

where e_i and e_j are the fracture apertures at intersection i and j.

Coupling DEM with Fluid Flow

The coupling between DEM and network fluid flow is governed by two-way feedback process: pressure gradient is used to calculate the exerted force on particles, and distribution of DEM particles is used to calculate the local porosity that feeds back to fluid flow model.

First, pressure gradient at the center of each DEM particle is interpolated according to hydraulic heads at fracture intersections. Second, the exerted force on particle due to fluid pressure is given as follows,

$$\begin{aligned}\vec{f}&=-\iint_{\Gamma}p\cdot\vec{n}d\Gamma\\&=\iiint_{\Omega}\nabla pd\Omega\\&=\iiint_{\Omega}\nabla\left(\rho_f gh\right)d\Omega\end{aligned}, \tag{13}$$

In turn, the location of particles determined by the DEM model are used to evaluate the local porosity of the DEM linked-cell within which a fracture intersection lies (see Figure 3).

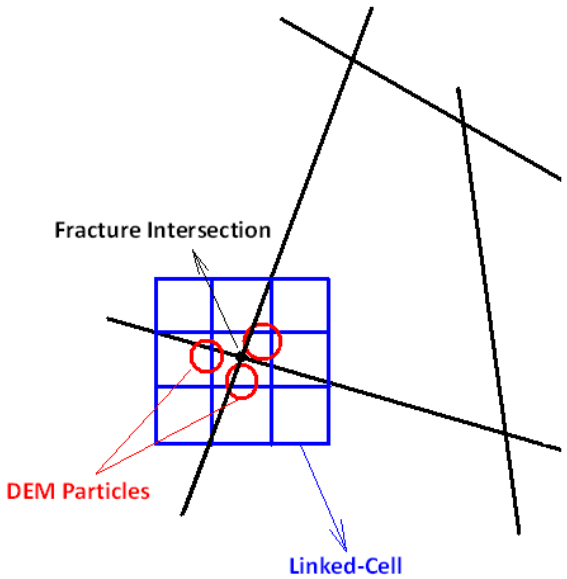

Figure 3: The schematic for computing local porosity from DEM particle locations

Numerical Algorithms

This section presents the methodology for implementing the governing equations of DEM, network flow, and coupling process, respectively.

DEM

Translational motion is governed by

$$F_i = m\left(\ddot{x}_i - g_i\right), \tag{14}$$

where F_i is the resultant force, the sum of all external applied forces acting on the particle; m is the total mass of the particle; g_i is the body force acceleration vector (e.g., gravity loading), $\ddot{x}_i$ is particle's acceleration.

The equation of rotational motion can be written in the vector form,

$$M_i = \dot{H}_i \left(= I\dot{\omega}_i = \left(\frac{2}{5} mR^2\right)\dot{\omega}_i \right), \tag{15}$$

where M_i is the resultant moment acting on the particle and H_i is the angular momentum of the particle; ω_i is the angular velocity of the particle.

The velocity verlet method (*Griebel, etc., 2007*) is implemented to solve the above equation. For each time step, it contains the following sub processes,

(1) Updating the particle location

$$x_i^{(t+\Delta t)} = x_i^{(t)} + \dot{x}_i^{(t)}\Delta t + \frac{1}{2}\ddot{x}_i^{(t)}\left(\Delta t\right)^2. \tag{16}$$

(2) Updating force and moment according to updated particle coordinates

$$x_i^{(t+\Delta t)} \Rightarrow F_i^{(t+\Delta t)}, M_i^{(t+\Delta t)} \Rightarrow \ddot{x}_i^{(t+\Delta t)} \tag{17}$$

(3) Updating the particle velocity by the following

$$\dot{x}_i^{(t+\Delta t)} = \dot{x}_i^{(t)} + \frac{1}{2}\left(\ddot{x}_i^{(t)} + \ddot{x}_i^{(t+\Delta t)}\right)\Delta t. \tag{18}$$

Network Flow Model

Collecting all equations at all intersections (including the ones at boundaries with known values of hydraulic heads) and moving the terms with known hydraulic heads into the right hand side (RHS) of the equation (*Jing and Stephansson, 2007*), one can obtain a simultaneous set of algebraic equations,

$$\left[T_{ij}\right]\left\{h_j\right\} = \left\{\hat{q}_i\right\}, \tag{19}$$

where the matrix $\left[T_{ij}\right]$ is called the global transmissivity matrix of the fracture system, essentially defining a cubic law between transmissivity of the fracture and its aperture size (see Equation 8),

$$T_{ii} = \frac{\rho_f g}{12\mu}\sum_{j=1}^{n_i}\frac{\left(e_{ij}\right)^3}{L_{ij}}, \tag{20}$$

and

$$T_{ij} = -\frac{\rho_f g}{12\mu}\frac{\left(e_{ij}\right)^3}{L_{ij}}, \quad (i \neq j, \text{ but } i \text{ and } j \text{ are adjacent intersections});$$

$T_{ij} = 0$, (i and j are not adjacent intersections).

The RHS vector $\left\{\hat{q}_i\right\}$ is given by

$$\hat{q}_i = q_i^s + \frac{\rho_f g}{12\mu}\sum_{k=1}^{n_i}\frac{\left(e_{ik}\right)^3}{L_{ik}}\hat{h}_k, \tag{21}$$

where $\hat{h}_k \left(k = 1, \cdots, n_i\right)$ are the known hydraulic heads at intersections k adjacent to intersection i.

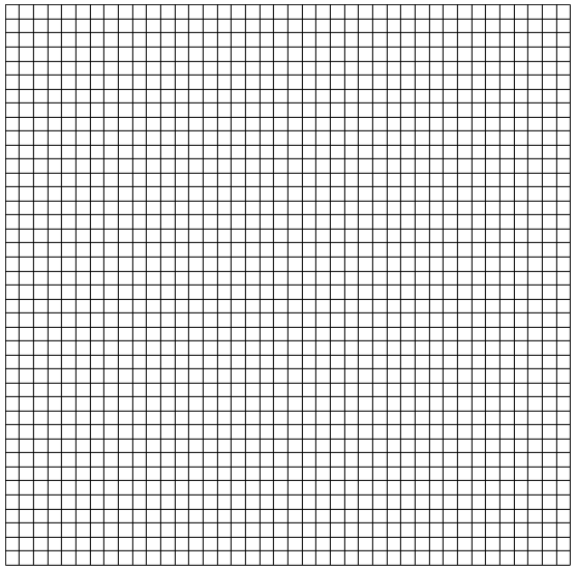

Figure 4: The initial fracture network with uniform aperture size

Coupling DEM with Fluid Flow

We extended the velocity verlet method (*Griebel, et al., 2007*) to simulate the coupling DEM with fluid flow. The extended method is applied as follows, in each time step.

(1) Calculate particle displacement and new location according to the velocity and acceleration at the end of the previous step;
(2) Calculate all current apertures and lengths of fracture segments according to updated particle coordinates;
(3) Calculate current hydraulic heads at all fracture intersections (assuming that fluid flow reaches steady state instantaneously);
(4) Calculate the external force due to fluid pressure of all particles;
(5) Calculate the interaction force between particles;
(6) Calculate acceleration of all particles according to the force of fluid pressure and interactions, and finally update all particles velocity.

Numerical Results

In order to demonstrate our proposed method, a synthetic case for DEM / network flow model coupling has been developed. In this example, all quantities are normalized by Young's Modulus, the average diameter of DEM particles, and time for elastic wave passing a mean diameter of DEM particles, respectively. The dimension of the simulation domain is $100\times100\times1$. The external boundaries are prescribed stress $\sigma_1 = \sigma_2 = 0.0005$ and fixed hydraulic heads ($h \equiv 0$). The rock matrix has an original regular fracture network and uniform aperture size of the average radius of DEM particles (see Figure 4). We inject water at the center of simulation zone at a pressure $p = 0.01$. In addition, the critical tensile and shear strain thresholds for cement bond breaking are set to $\varepsilon^t = 0.001$ and $\varepsilon^s = 0.001$, respectively. Particle radius, Young's Modulus and strain thresholds are perturbed by random number that satisfies a uniform distribution of 0.94 ~ 1.06.

Following the assumption of the permeability in the rock matrix being significantly smaller than the permeability of the fractures, the fluid flow in the rock matrix is negligible. Figures 5 and 6 show the hydraulic heads at the end of the first time step's injection.

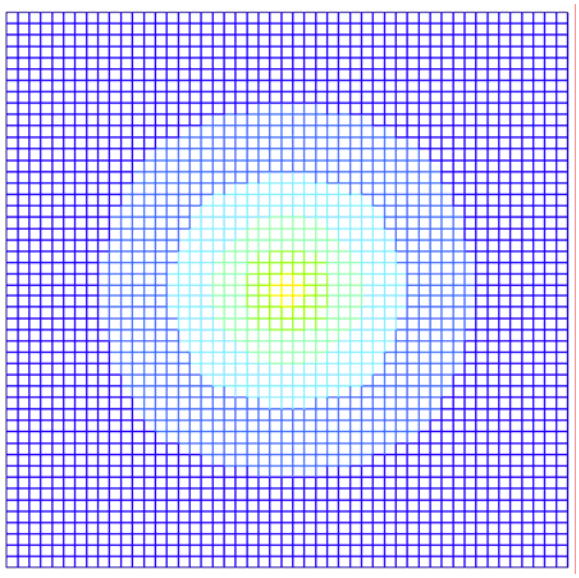

Figure 5: The hydraulic heads at the fracture intersection at the end of the first time step's injection, prior to matrix/fracture network deformation.

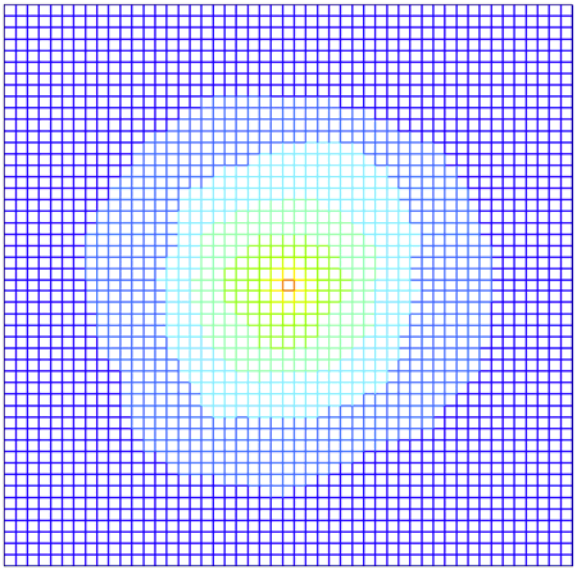

Figure 6: The final hydraulic heads

Figures 7 and 8 show the typical DEM particle movement. For all particles, movement is driven by pressure gradient. For homogeneous media particle displacement should be symmetric, but in this example the slight randomization of the property distributions allow for more robust behavior to be predicted.

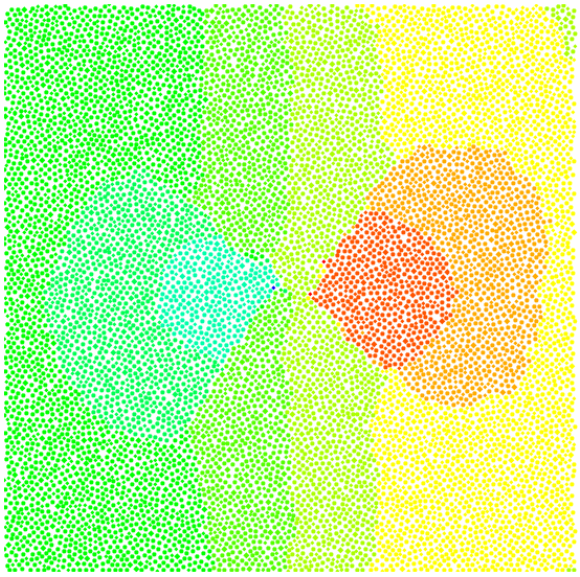

Figure 7: Contour of x-displacement (time=300)

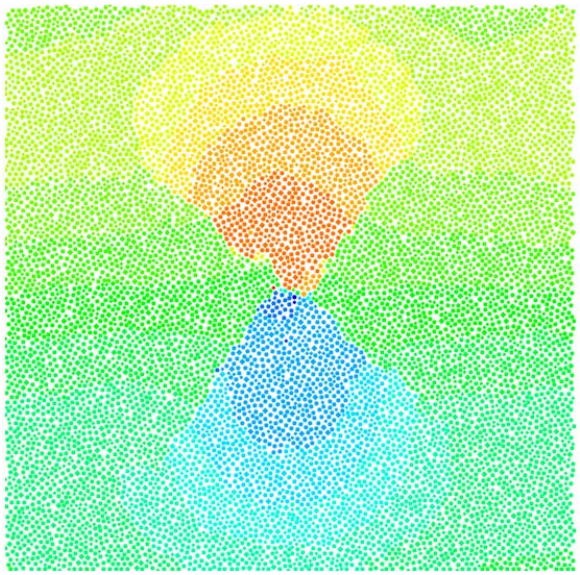

Figure 8: Contour of y-displacement (time=300)

Figures 9 and 10 show the intermediate (time is 300) and final cement bond status (time is 600), respectively. Blue indicates unbroken bonds; yellow and red indicate tension-induced and shear-induced breaks, respectively. From Figures 9 and 10, we can see that the hydraulic fracturing is dominated by shear-induced failure; tension can also play an important role in hydraulic fracturing however, if all boundaries are extraction free. In addition, the boundary conditions can also affect the ultimate result, e.g. propagation angle of fractures. In this example, the fracture angle is approximately 45^{o}, aligned with the maximum shear stress along these directions.

As would be expected, hydraulic fracturing is initiated near the injection location and propagates outward as the status of the cement bond reaches / exceeds the pre-specified failure criteria. Moreover, the fracturing zone always lies in the zone with the maximum gradient of hydraulic head, and it propagates, following the leading edge of failure during hydraulic fracturing process.

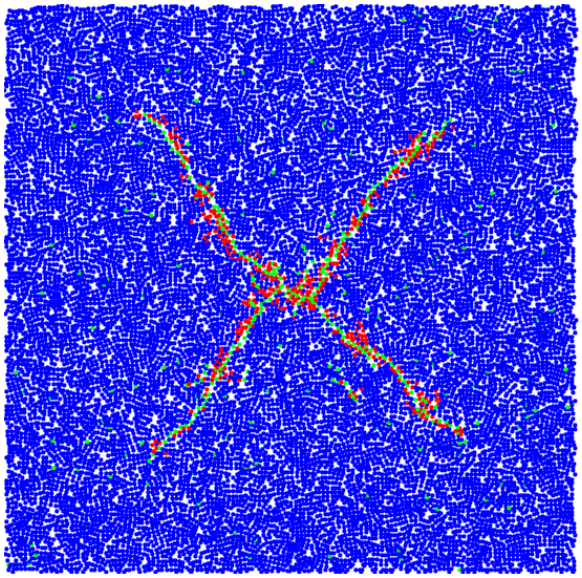

Figure 9: The intermediate bond status. Each point represents the center of a cement bond.

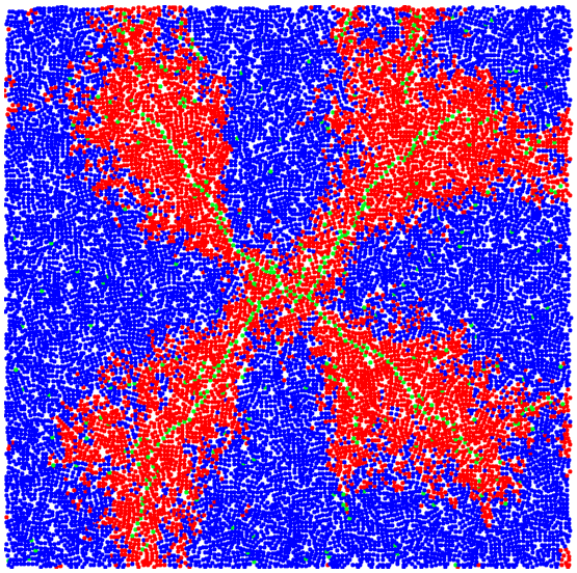

Figure 10: The final bond status. Each point represents the center of a cement bond.

For evaluating the aperture and permeability, and their evolution, we choose the following 2 equations to calculate the average aperture and permeability at each time step,

$$\tilde{e} = \frac{\sum_{i=1}^{n}\sum_{j=1}^{n_i}\left(e_{i,j,1}+e_{i,j,2}\right)}{\sum_{i=1}^{n}\sum_{j=1}^{n_i}\left(e^0_{i,j,1}+e^0_{i,j,2}\right)}, \qquad (22.a)$$

and

$$\tilde{k} = \frac{\sum_{i=1}^{n} k_i}{\sum_{i=1}^{n} k_i^0}, \qquad (22.b)$$

where, n is the number of fracture intersections, $e^0_{i,j,1}$ and $e^0_{i,j,2}$ are the initial aperture sizes at the ends of the fracture segment between the *i*th and *j*th intersection, $e_{i,j,1}$ and $e_{i,j,2}$ are the current aperture sizes at the ends of the fracture segment between the *i*th and *j*th intersection. k_i^0 and k_i are the initial and current permeability at the *i*th intersection. The results are shown on Figure 11 and Table 1. One can see that the aperture sizes and permeability are predicted increase as the rock matrix blocks are fractured and the fracture network is dilated due to fluid pressure increases.

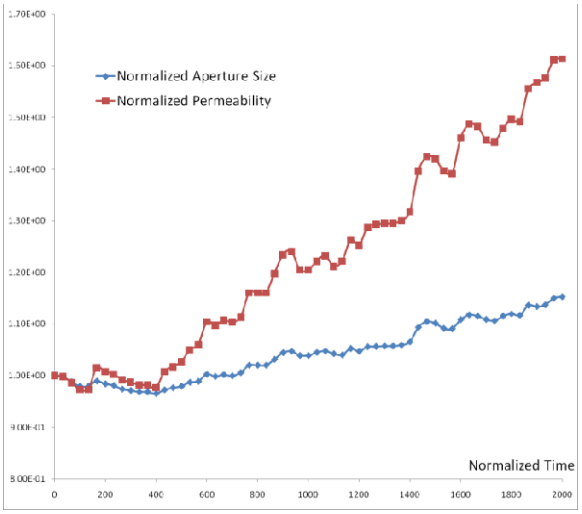

Figure 11: The evolution of the normalized average aperture size and permeability with time

Table 1 gives the normalized values of the initial and final (average) aperture sizes and permeability.

Table 1: The initial and final normalized aperture sizes and permeability

	Initial Value	**Final Value**
Aperture Size	1.0	1.15
Permeability	1.0	1.61

Conclusion

In this paper, we proposed and implemented a coupling method for DEM and network flow models. In the method, water primarily flows in the fracture networks. Fluid pressures within the rock matrix are interpolated linearly from the surrounding fracture network, and are only used to propagate the force (and resultant deformation/fracturing) throughout the rock matrix.

The deformation and fracturing of the rock are modeled by DEM, with rock motion and fracturing being represented by particle movement and cement bond breakage between particles. In the coupled model, particle displacement is driven by fluid pressure gradient, which changes the local porosity and ultimately the fracture aperture. Conversely, the changes of the aperture sizes will affect the hydraulic head distribution and provide feedback to change the exerted force on each particle-which is the coupling process.

The preliminary results demonstrate that the proposed method has the ability to simulate the interactions between fluid flow and rock deformation and fracturing. Our preliminary results show that the model predicts: (i) boundary conditions affect the fracturing mode (though the fracturing angle is near $45^{o)}$, (ii) fracturing occurs in the areas with the maximum gradient of hydraulic head and it moves during hydraulic fracturing. While these results are encouraging and give some confidence with the modeling methods, there are a number of significant improvements that need to be made. The fluid model is overly simplistic and is not compatible with our

transient three-dimensional DEM code (as implemented it is for steady state conditions only).

Future work includes two general areas, with the first being to verify the presented method further, and the second to implement a more sophisticated flow model to handle transient interaction process between fluid flow and rock deformation / fracturing (e.g. Darcy's Law).

References

Bear, J. (1992), "Modeling flow and contaminant transport in fractured rocks" in "*Flow and Contaminant Transport in Fractured Rock (Edited by Bear J., Tsang C.F. and Marsily G.)*", Academic Press.

Griebel M., Knapek, S., and Zumbusch, G. (2007), Numerical Simulation in Molecular Dynamics – Numerics, Algorithms, Parallelization, Applications, Springer.

Jing, L. and Stephansson, O. (2007), Fundamentals of discrete Element Methods for Rock Engineering: Theory and Applications, Elsevier

Potyondy, D.O. and Cundall, P.A. (2004), "A bonded-particle model for rock", "*International Journal of rock Mechanics & Mining Sciences*", **41**, 1329 – 1364.

Steefel, C.I. and Lasaga, A.C. (1994), "A coupled model for transport of multiple chemical species and kinetic precipitation/dissolution reactions with applications to reactive flow in single phase hydrothermal system", "*Am. J. Sci.*", 294, 529-592.